Cerebral Cortex, March 2021;31: 1719–1731

doi: 10.1093/cercor/bhaa321
Advance Access Publication Date: 14 November 2020
Original Article

ORIGINAL ARTICLE

Atlas55+: Brain Functional Atlas of Resting-State Networks for Late Adulthood

Gaelle E. Doucet[1,2], Loic Labache[3], Paul M. Thompson[4], Marc Joliot[3], Sophia Frangou[2,5] and for the Alzheimer's Disease Neuroimaging Initiative[†]

[1]Boys Town National Research Hospital, Omaha, NE 68131, USA, [2]Department of Psychiatry, Icahn School of Medicine at Mount Sinai, New York, NY 10029, USA, [3]GIN, UMR5293, CEA, CNRS, Bordeaux University, Bordeaux 33000, France, [4]Imaging Genetics Center, Mark and Mary Stevens Neuroimaging and Informatics Institute, Keck School of Medicine, University of Southern California, Marina del Rey, CA 90033, USA and [5]Centre for Brain Health, University of British Columbia, Vancouver, BC, V6T 1Z4, Canada

Address correspondence to Gaelle Doucet, Brain Architecture, Imaging and Cognition Lab, Boys Town National Research Hospital, 555 N 30th street, Omaha, NE 68131, USA. Email: gaelle.doucet@boystown.org.

[†]Data used in preparation of this article were obtained from the Alzheimer's Disease Neuroimaging Initiative (ADNI) database (adni.loni.usc.edu). As such, the investigators within the ADNI contributed to the design and implementation of ADNI and/or provided data but did not participate in analysis or writing of this report. A complete listing of ADNI investigators can be found at: http://adni.loni.usc.edu/wp-content/uploads/how_to_apply/ADNI_Acknowledgement_List.pdf

Abstract

Currently, several human brain functional atlases are used to define the spatial constituents of the resting-state networks (RSNs). However, the only brain atlases available are derived from samples of young adults. As brain networks are continuously reconfigured throughout life, the lack of brain atlases derived from older populations may influence RSN results in late adulthood. To address this gap, the aim of the study was to construct a reliable brain atlas derived only from older participants. We leveraged resting-state functional magnetic resonance imaging data from three cohorts of healthy older adults (total $N = 563$; age = 55–95 years) and a younger-adult cohort ($N = 128$; age = 18–35 years). We identified the major RSNs and their subdivisions across all older-adult cohorts. We demonstrated high spatial reproducibility of these RSNs with an average spatial overlap of 67%. Importantly, the RSNs derived from the older-adult cohorts were spatially different from those derived from the younger-adult cohort ($P = 2.3 \times 10^{-3}$). Lastly, we constructed a novel brain atlas, called Atlas55+, which includes the consensus of the major RSNs and their subdivisions across the older-adult cohorts. Thus, Atlas55+ provides a reliable age-appropriate template for RSNs in late adulthood and is publicly available. Our results confirm the need for age-appropriate functional atlases for studies investigating aging-related brain mechanisms.

Key words: aging, brain functional atlas, late adulthood, resting-state networks

Introduction

Resting-state functional magnetic resonance imaging (rs-fMRI) has been instrumental in mapping the brain functional connectome in health (Fox et al. 2005; Smith et al. 2009; Doucet et al. 2011; Smith et al. 2015) and disease (Feltz and Miller 1996; Buckner et al. 2009; Tracy and Doucet 2015; Doucet et al. 2017; Dong et al. 2018; Sha et al. 2019). The brain functional connectome can be defined as a multiscale partition in which regions may be aggregated into networks, which in turn may be combined into larger systems (Kiviniemi et al. 2009; Abou Elseoud et al. 2011; Doucet et al. 2011). Previous work by us and others suggest that the intermediate partition of the brain

at the level of networks may be optimal to explain cognitive activity and to identify reliable biomarkers of neuropsychiatric and neurological disorders (van den Heuvel and Hulshoff Pol 2010; Abou Elseoud et al. 2011; Doucet et al. 2011; Doucet et al. 2012; Doucet et al. 2017; Salman et al. 2019), while limiting multiple comparisons when compared to finer brain partitions (Zalesky et al. 2010). At this level of brain organization, five major resting-state networks (RSNs) and their subdivisions have been typically identified across rs-fMRI studies: those involved in internally guided, higher order mental functions as part of the intrinsic system (default mode [DMN], executive control [ECN], and salience [SAL] networks) and those supporting externally driven, specialized sensory and motor processing as part of the extrinsic system (visual [VIS] and sensorimotor [SMN] networks) (De Luca et al. 2006; Smith et al. 2009; Doucet et al. 2011; Buckner et al. 2013; Doucet et al. 2019). Each of these brain networks relies on established white matter (WM) pathways (Toosy et al. 2004; Greicius et al. 2009; van den Heuvel et al. 2009) that support the consistency of their spatiotemporal configuration and functional roles (Damoiseaux et al. 2006; Smith et al. 2009; van den Heuvel and Hulshoff Pol 2010; Doucet et al. 2011; Doucet et al. 2019; Elliott et al. 2019).

Several brain functional atlases are currently available which support reproducibility by harmonizing the RSN definition across neuroimaging studies (Doucet et al. 2019). However, to date, the only brain functional atlases available are derived from samples of young healthy adults, typically below the age of 40 years (Doucet et al. 2019). Nonetheless, changes in brain function over the course of adulthood have been well-documented and suggest that brain networks are continuously reconfigured throughout adult life (Damoiseaux et al. 2008; Meunier et al. 2009; He et al. 2013; Betzel et al. 2014; Damoiseaux 2017; Varangis, Razlighi, et al. 2019b; Yaple et al. 2019; Luo, Sui, Abrol, Lin, et al. 2020b). To our knowledge, there is currently no reference brain functional atlas derived from rs-fMRI data from older adults, and this may undermine neuroimaging efforts to characterize the brain functional connectome and its cognitive role in late adulthood. Critically, differences in the spatial composition of the RSNs derived from large samples of younger versus older adults have yet to be systematically investigated.

In this context, the current study focused on the spatial definition of the five major RSNs (DMN, ECN, SAL, VIS, and SMN) and their subdivisions in healthy adults aged 55 years and older. The specific aims were: (1) to test the reproducibility of RSNs in three large independent cohorts comprising a total of 563 older healthy adults (age range: 55–95 years); accordingly, we analyzed data from the Center for Aging and Neuroscience (CamCAN) project (Shafto et al. 2014; Taylor et al. 2017), the Southwest University Adult Lifespan Dataset (SALD) (Wei et al. 2018) and the Alzheimer's Disease Neuroimaging Initiative (ADNI) database (Jack Jr. et al. 2008; Petersen et al. 2010); (2) to identify differences in the anatomical constitution of RSNs defined in the above cohorts compared to those in younger adults (age range 18–35); and (3) generate a reliable consensual RSN atlas to enhance the reproducibility of template-defined RSNs in older adults.

Materials and Methods

Cohorts

Older-Adult Cohorts

We used data from the CamCAN (Shafto et al. 2014; Taylor et al. 2017), the SALD (Wei et al. 2018) and the ADNI datasets (Jack Jr. et al. 2008; Petersen et al. 2010). In each cohort, we selected healthy individuals aged 55 years and above for whom both rs-fMRI and structural MRI data were available. This selection resulted in a sample of 250 individuals for CamCAN (referred to as "CamCAN55+"), 190 for SALD, and 134 for ADNI (details in supplementary material). Following quality control of the imaging data (described below), 11 participants across cohorts were removed for excessive head motion. The total analysis sample for the older individuals comprised 563 individuals, described in Table 1 and Supplementary Figure S1.

Younger-Adult Cohort

A subset of the CamCAN cohort, referred to as "CamCAN35-", was used to test for differences between younger (18–35 years old) and older (55 years and older) adults in RSN spatial composition. This age range was chosen to match the typical age range of healthy participants used in currently available functional atlases (Doucet et al. 2019). The CamCAN35− included 128 individuals. Following the same quality control process, we excluded two individuals from CamCan35− (Table 1).

Resting-State fMRI Acquisition and Preprocessing

In the CamCAN cohort, rs-fMRI data were acquired while participants rest with their eyes closed on a 3 T Siemens TIM Trio scanner with a 32-channel head coil with the following acquisition parameters: TR/TE = 1970/30 msec, 32 axial slices, flip angle =78°; FOV =192 mm × 192 mm; voxel-size = 3 mm × 3 mm × 4.44 mm, acquisition time = 8 min 40 sec, number of volumes: 261. More information on the MRI sequences can be found in Taylor et al. (2017).

In the SALD cohort, rs-fMRI data were acquired while participants rest with their eyes closed on a 3 T Siemens Trio scanner, using the following acquisition parameters (Wei et al. 2018): TR/TE = 2000/30 msec, 32 axial slices, flip angle = 90°; FOV = 220 mm × 220 mm; voxel-size = 3.4 mm × 3.4 mm × 4 mm, acquisition time = 8 min, number of volumes: 242. More information on the MRI sequences can be found in Wei et al. (2018).

In the ADNI cohort, rs-fMRI data were acquired while participants kept their eyes open. Acquisition tool place in 43 sites using 3 T scanners (General Electric [GE], Philips or Siemens) and variable acquisition protocols (details in http://adni.loni.usc.edu/methods/documents/) that commonly used a TR = 3000 sec, with 140–200 volumes. When multiple resting-state fMRI datasets were available for a participant, the first one was selected for analyses.

Regardless of the cohort, the rs-fMRI data were preprocessed in an identical fashion, using SPM12 and the DPABI Toolbox (Yan et al. 2016). Preprocessing procedures for the rs-fMRI datasets included removal of the first three volumes, motion correction to the first volume with rigid-body alignment; coregistration between the functional scans and the anatomical T1-weighted scan; spatial normalization of the functional images into Montreal Neurological Institute stereotaxic standard space; spatial smoothing within the functional mask with a 6-mm at full-width at half-maximum Gaussian kernel; wavelet despiking (Patel et al. 2014); linear detrending; and regression of motion parameters and their derivatives (24-parameter model) (Friston et al. 1996), as well as WM, CSF time series. The WM and CSF signals were computed using a component based noise reduction method (CompCor, 5 principal components) (Behzadi et al. 2007). Lastly, bandpass filtering was applied at 0.01–0.1 Hz (Cordes et al. 2001).

Table 1 Cohort characteristics

Cohort	*N*	Age, years (mean (SD))	Age range (years)	Sex (% females)	rs-fMRI TR (sec)	rs-fMRI volumes	rs-fMRI instruction
CamCAN55+	246	71.3 (9.3)	55–88	49%	1.97	261	Closed eyes
SALD	185	63.1 (6.5)	55–80	61%	2.00	242	Closed eyes
ADNI	132	78.9 (7.0)	62–95	50%	3.00	140–200*	Open eyes
CamCAN35−	128	28.4 (4.8)	18–35	58%	1.97	261	Closed eyes

CamCAN, Cambridge Center for Ageing and Neuroscience; SALD, Southwest University Adult Lifespan Dataset; ADNI, Alzheimer's Disease Neuroimaging Initiative; TR, repetition time; rs-fMRI; resting-state functional magnetic resonance imaging sequence.
*Number of volumes vary by ADNI site, see detail in supplementary material.

As previously mentioned, across the three older-adult cohorts, we excluded 11 individuals who had excessive head movement based on maximum transient (volume-to-volume) head motion above 2 mm translation or 1° rotation. After removing these individuals, we ensured that head motion, based on the mean framewise displacement (Power et al. 2012) did not correlate with age ($r = 0.08$). Following the same process, we excluded two individuals from the CamCan35− cohort.

Resting-State Networks in the Older-Adult Cohorts

Resting-State Networks Identification in the Older-Adult Cohorts

We used a process validated by Naveau et al. (2012) to identify reliable brain networks. First, for each individual within each cohort, single-subject independent component analyses (ICAs) were conducted 20 times with random initialization using the Multivariate Exploratory Linear Optimized Decomposition into Independent Components software, version 3.15, included in the FMRIB Software Library (FSL) v6.0.3 (http://www.fmrib.ox.ac.uk/fsl) (Smith et al. 2004). The number of independent components (ICs) was estimated by Laplace approximation (Minka 2000). A symmetric approach of the FastICA algorithm (Hyvarinen 1999) was used to compute the ICAs. Second, for each repetition, we used the multiscale clustering of individual component algorithm (MICCA) to classify ICs into *N* groups (Naveau et al. 2012). The number of groups was automatically estimated by the algorithm (Naveau et al. 2012). Third, the *Icasso* algorithm (Himberg et al. 2004) was used to select groups of reproducible ICs (i.e., groups with ICs that were present in at least 50% of the 20 repetitions), which we identified as the "group-level components" (Salman et al. 2019). Fourth, for each group-level component, a voxel-wise *t*-score map of individual ICs was computed and thresholded using a mixture model ($P > 0.95$, (Beckmann and Smith 2004)). Lastly, we discarded group-level components if their spatial map: (1) mainly covered nongray matter (i.e., CSF and WM), or (2) included regions with strong signal attenuation due to susceptibility artifacts (i.e., lower frontal and lower temporal regions) (Supplementary Figs. S2–S4).

Spatial Overlap of Group-Level Components in Older-Adult Cohorts

Within each cohort, we mapped the spatial overlap across the group-level components by computing an index that quantified the number of group-level components overlapping at each voxel. This voxel-wise index ranged from 1 (no spatial overlap, the voxel is assigned to only one component) to *n* (where *n* is the maximum number of components overlapping at a voxel).

As the goal of the current study was to create a reliable functional atlas of RSNs, we created nonoverlapping group-level components, on which we based the remaining analyses. Accordingly, each brain voxel was assigned to the group-level components with the highest *t*-score.

Reliability Analyses of the Group-Level Components in Older-Adult Cohorts

As the spatial configuration of a brain network is strongly related with its functional connectivity (Bijsterbosch et al. 2018), we conducted supplementary analyses to assess the functional reliability of each group-level component, in each cohort, following the methods described in Labache et al. (2020) (Supplementary Fig. S5). In each cohort, we generated a dendrogram based on the average connectivity matrix between the group-level components. The functional reliability of a group-level component depended on the number of times it maintained the same position in the dendrogram of each individual participant of the same cohort. We created a reliability index (Q) for each group-level component, where a score close to zero indicated perfect functional reliability and a high score indicated high functional unreliability (details in supplementary information and Supplementary Fig. S5). We conducted Tukey's fences tests to identify and discard these highly unreliable group-level components.

Construction of the Major RSNs in Older-Adult Cohorts

We chose to focus on the major RSNs defined as: the DMN, the ECN, the SAL, the SMN, and the VIS (Smith et al. 2009; Doucet et al. 2011; Doucet et al. 2019) and their subdivisions and examined their spatial definition across the three cohorts.

Following the identification of nonoverlapping and functionally reliable group-level components in each cohort, we proceeded to assigning them to the major RSNs of interest, namely the DMN, ECN, SAL, VIS, and SMN. As reference for each network, we used their spatial definition in the Consensual Atlas of REsting-state Networks (CAREN) (Doucet et al. 2019). This atlas was generated by our group and presents the spatial configuration of the major RSNs based on their common properties across the most widely used brain functional atlases and as such it represents the most reproducible spatial features of the major RSNs currently available. This choice was also based on the fact that, to the best of our knowledge, there are currently no validated and reproducible RSNs from rs-fMRI data of a large sample of older healthy individuals that we could use as normative templates.

In each cohort, we computed the Dice coefficient (Dice 1945) to quantify the degree of spatial overlap between each group-level component and each of the five aforementioned CAREN RSNs. Components were then assigned to the RSN with which they had the largest overlap (Supplementary Table S1). We applied this process to each cohort separately to create spatial maps of the major RSNs. We were thus able to construct

a spatial map for each RSN. We used the Dice coefficient to test the pairwise similarity between the same-labeled RSNs across cohorts. Lastly, to ensure that the results did not depend on the template used (i.e., CAREN), we also used the atlas created by Yeo et al. (2011) for the RSN assignment.

Spatial Comparison of the Major RSNs Between Young and Older Adults

Prior to testing for differences in the spatial constitution of RSNs between older and younger adults we constructed the major RSNs in the CamCAN35− by applying the same procedure as for the older cohorts (Supplementary Fig. S12).

We then compared their respective RSNs to those derived from the other two independent cohorts (ADNI and SALD). For this, we used Dice's coefficient to quantify the spatial similarity of the RSNs in CamCAN35−, and in CamCAN55+ respectively, to those of SALD and ADNI, and compared these pairwise coefficients (i.e., we compared the coefficients resulting from the RSN comparison CamCAN55+ vs. SALD and ADNI to those resulting from the RSN comparison CamCAN35− vs. SALD and ADNI). This choice of approach was based on two major reasons: (1) among the three cohorts, CamCAN was the largest and also provided more reliable data (having the largest number of rs-fMRI volumes (Elliott et al. 2019), Table 1); and (2) this approach enabled us to account for differences in analytic approach, site, and MRI acquisition parameters.

Generation of Atlas55+

The major RSNs identified in each of the three older-adult cohorts were used as input data to create a consensual atlas, named Atlas55+. For this, we used the function *consensus_similarity.m* from the Network Community Toolbox (http://commdetect.weebly.com), which constructs a representative partition.

To test the spatial reproducibility of the major RSNs in Atlas55+, we conducted supplementary analyses: (1) we assigned each brain voxel to a network only if at least two of the three older-adult cohorts assigned this voxel to the same network. We then computed a spatial correlation between the two versions of Atlas55+ using Pearson's correlation analyses. (2) We created a voxel-wise confidence map to quantify the consistency of the network assignment between the RSNs of the atlas and those from each of the three older-adult cohorts. This voxel-wise index ranged from 0 (poor confidence, the network assignment of a voxel in Atlas55+ differed from its network assignment in all three cohorts) to 100% (high confidence, the network assignment of a voxel in Atlas55+ was identical to its network assignment in all three cohorts). Lastly, we compared the RSNs of the atlas to those of CamCAN35− in order to quantify the spatial differences between RSNs from younger adults and older adults, computing Dice coefficients.

To identify the anatomical definition of each major RSN in the atlas, we generated subject-specific versions using a dual regression approach in FSL (Beckmann et al. 2009; Nickerson et al. 2017). We then entered each network into a one-sample *t* test, adding age, head motion (mean framewise displacement), estimated total intracranial volume (TIV, measured using FreeSurfer v6.0 (http://surfer.nmr.mgh.harvard.edu/)), and site as covariates of no interest. Significant regions were reported at a $P < 0.05$ after applying a family wise error (FWE) correction at the voxel level ($T > 5.3$, cluster size > 20 voxels).

Subdivisions of the RSNs within Atlas55+

We then focused on the subdivisions of each RSN within Atlas55+ to increase the spatial resolution of the atlas across the three older-adult cohorts.

For each major RSN, we quantified the degree of spatial overlap between the group-level components assigned to that RSN across the three cohorts, using Dice coefficients (Supplementary Table S1). Based on these coefficients, we constructed a dendrogram and identified clusters with high spatial overlap across independent group-level components, with one component from each of the three cohorts (Supplementary Fig. S11). Lastly, we created a spatial map for each of these clusters, which displays the spatial characteristics of a subdivision of that RSN (Supplementary Table S3). A voxel was identified as part of that RSN subdivision if it was found in at least two out of the three components. We chose to focus on clusters with contributions from all three older-adult cohorts because this suggests that these components were reliably found in each cohort and therefore were minimally influenced by acquisition parameters.

Effects of Sex and Age on the Major five RSNs in the Atlas55+

The effect of age on the spatial distribution of each major RSN in the atlas (extracted from the dual regression) across all individuals (total $n = 563$) was tested by conducting an analysis of covariance, adding covariates of no interest: head motion, TIV, and site. Sex differences in the spatial distribution of the RSNs in the atlas were also assessed using age, head motion, TIV, and site as covariates of no interest. Significant clusters are reported at a $P < 0.05$ with FWE correction at the voxel level ($T > 5.3$, cluster size > 20 voxels).

Results

Identification of Group-Level Components in the Older-Adult Cohorts

In the CamCAN55+, SALD and ADNI cohorts, we respectively identified a total of 27, 24 and 23 reproducible group-level components (Supplementary Figs. S2–S4 and S8). For the CamCAN55+ cohort, we found that 27% of the voxels were assigned to a single group-level component, whereas less than 0.5% of the voxels were assigned to a maximum of nine group-level components. The degree of spatial overlap between components was similar for the other two cohorts (Supplementary Fig. S7). Regardless of cohort, the regions with the highest overlap were located in the medial posterior cortex, the dorso-medial prefrontal cortex and the lateral parietal cortex (Supplementary Fig. S7).

Regardless of cohort, the functional reliability tests showed that all group-level components had a similar degree of stability, with no outlier, across individuals and in each cohort (Supplementary Fig. S6). The reliability Q scores of each component did not differ across cohorts ($P > 0.1$).

Construction and Reliability of the Major RSNs in the Older-Adult Cohorts

The five RSNs constructed in each older-adult cohort (Fig. 1) showed high spatial reproducibility across the three cohorts with an average spatial overlap of 67% (mean range: 66–69%), with the SAL having the lowest score (46%) and the VIS having

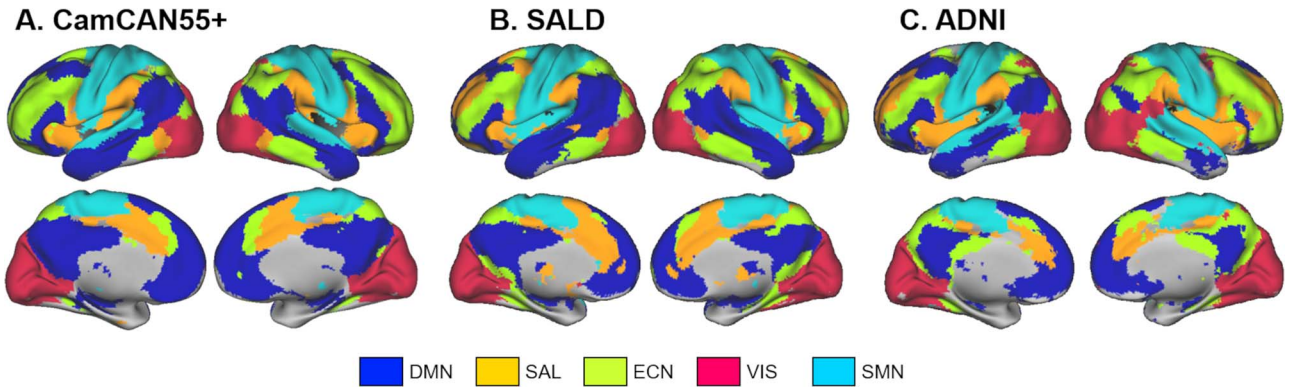

Figure 1. Spatial map of the five major RSNs. (*A*) CamCAN55+, (*B*) SALD, and (*C*) ADNI. DMN, default mode network; SAL, salience network; ECN, executive control network; VIS, visual network; SMN, sensorimotor network.

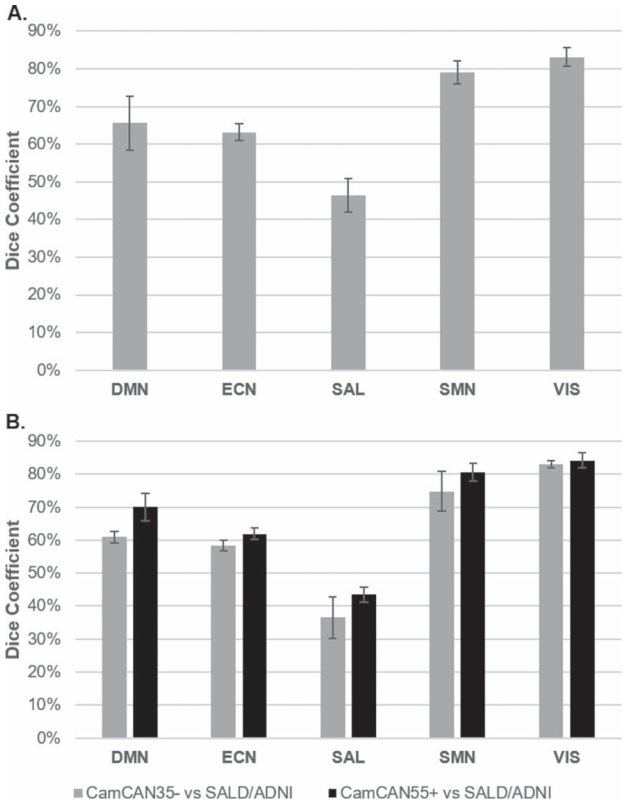

Figure 2. Spatial similarity of the RSNs across the cohorts. (*A*) Spatial similarity of the RSNs across the older-adult cohorts. (*B*) Comparison of the spatial similarity of the RSNs identified in the CamCAN35− versus the ADNI and SALD cohorts and in the CamCAN55+ versus the ADNI and SALD cohorts. DMN, default mode network; SAL, salience network; ECN, executive control network; VIS, visual network; SMN, sensorimotor network.

the highest score (83%) (Fig. 2A). Supplementary Figure S9 shows the voxel-wise confidence values with respect to the probability of a voxel being assigned to the same-labeled RSN across the three cohorts. The majority of voxels (83.5%) had confidence values over 66%, indicating that at least two out of the three cohorts had the same RSN assignment.

The choice of a reference atlas, CAREN or Yeo, minimally affected the spatial definition of the RSNs. The average spatial overlap of each RSN constructed based on CAREN versus each RSN constructed based on Yeo's atlas was 86% across the three cohorts (CamCAN: 86% (sd = 15%), SALD: 85% (19%), ADNI: 86% (9%); Supplementary Fig. S10).

Comparison of the Major RSNs between Older- and Young Adults

We found that the major RSNs in the CamCAN35− (Supplementary Fig. S12) were less similar to those identified in the SALD and ADNI than in the CamCAN55+ ($t = -4.2$, $P = 2.3 \times 10^{-3}$; Fig. 2B). The SMN and VIS, which cover primary cortices differed the least, whereas the SAL network showed the largest spatial difference between the younger and older cohorts.

Atlas55+

Atlas55+ is available at two resolution levels: at the lever of the five major RSNs (DMN, ECN, SAL, SMN, and VIS, Fig. 3A) and at the level of their 15 subdivisions that were also reliably identified across the three older-adult cohorts (Fig. 4). The anatomical description of each RSN and their subdivisions is detailed in Supplementary Tables S2 and S3. The degree of confidence in network assignment in Atlas55+ was high across the three older-adult cohorts (Fig. 3B). The SMN and VIS were the most reproducible networks with 77% and 93% of their voxels, respectively being consistently assigned across all three cohorts.

As defined in Atlas55+, the SMN was comprised of the sensory and motor regions (precentral and postcentral gyrus and supplementary motor area), the primary auditory cortex (superior temporal cortex), and thalamus. The SMN was further partitioned into four subdivisions: the ventral and dorsal parts of the pre- and postcentral gyri, the supplementary motor area and the bilateral superior temporal gyri (auditory network). The VIS network largely covered the occipital lobe, and was partitioned into two subdivisions: the medial and posterior parts (Fig. 4). Both SMN and VIS networks showed the largest spatial overlap with their respective networks in younger adults as outlined in CamCAN35− (spatial overlap: 69% and 84%, respectively; Fig. 5).

For the DMN, 51% of the network's voxels showed consistency across all three older-adult cohorts. In Atlas55+, the DMN comprised the medial prefrontal cortex/ventral anterior cingulate cortex (ACC), the precuneus/posterior cingulate cortex (PCC), the inferior frontal cortex, the angular gyri, the middle temporal cortex, the hippocampi and amygdala, and some

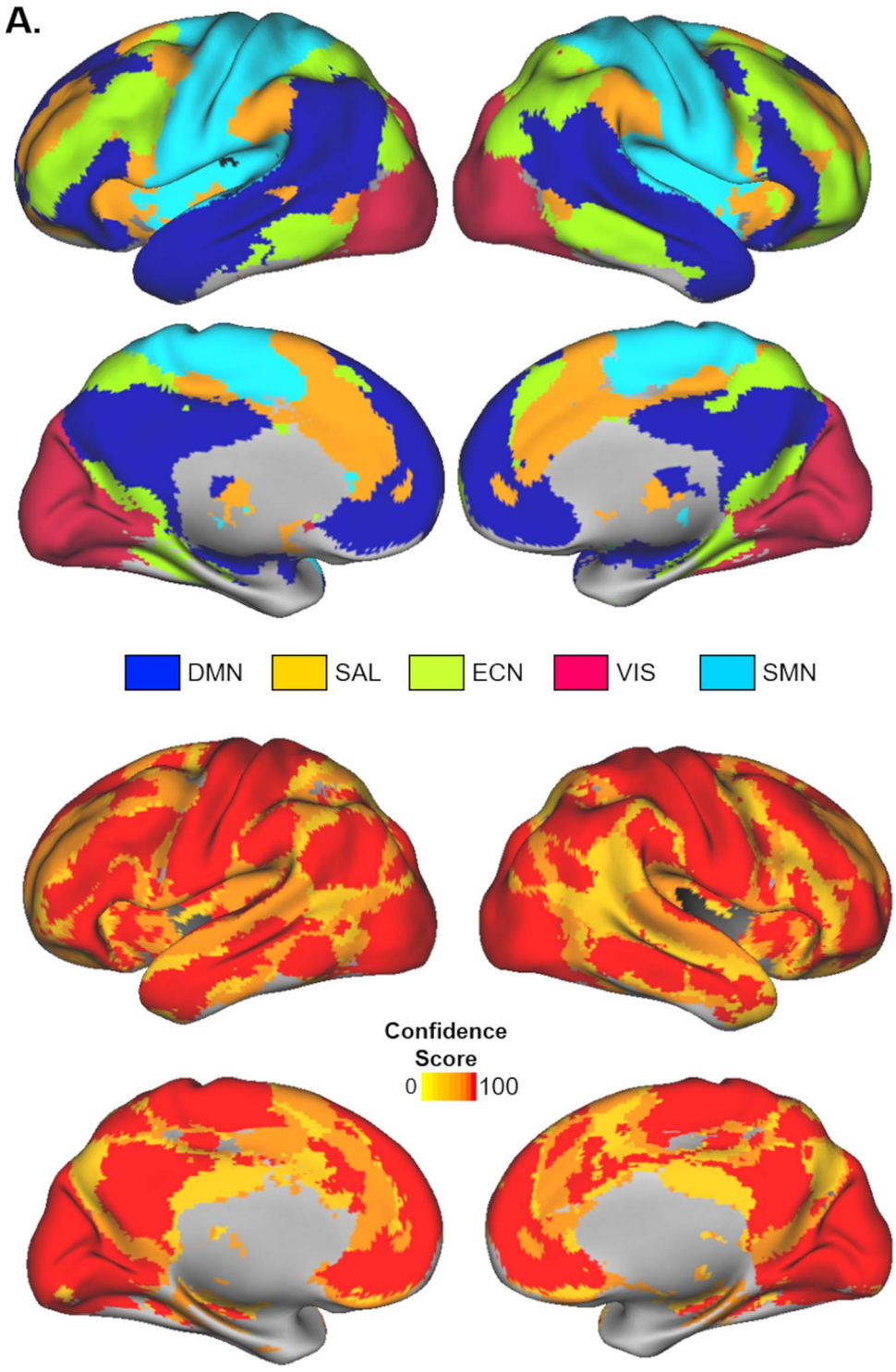

Figure 3. Atlas55+: consensus brain atlas composed of the five major resting-state networks based on three cohorts of healthy individuals aged 55 years and above. (*A*) Spatial map of the RSNs. (*B*) Voxel-wise confidence map in Atlas55+. This measure quantifies the probability that a voxel in an Atlas55+ network is assigned to the same-label RSN in each of the three cohorts. DMN, default mode network; SAL, salience network; ECN, executive control network; VIS, visual network; SMN, sensorimotor network.

bilateral cerebellar clusters. The DMN further included four reliable subdivisions comprising the anterior DMN (ACC), the core DMN (precuneus/PCC, medial prefrontal cortex, bilateral angular gyri), and two left lateralized networks mostly covering the inferior frontal gyrus, temporal poles and the posterior part of the superior temporal gyrus, and dorsal medial prefrontal cortex (Fig. 4). The whole DMN showed a 63% overlap with the DMN in younger adults as defined in CamCAN35− (Fig. 5). The

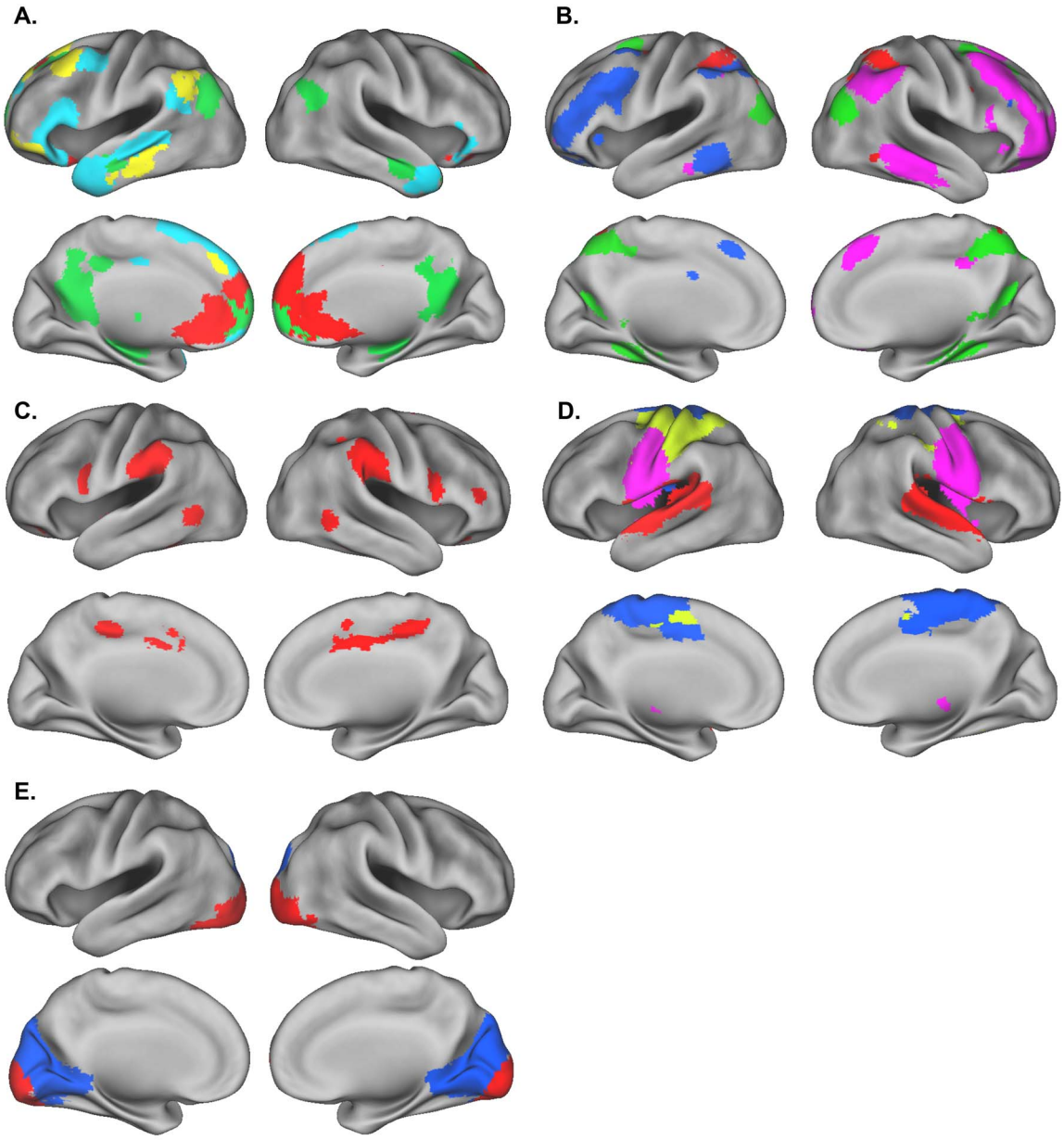

Figure 4. Reliable subdivisions of each of the five major RSNs across the three older-adult cohorts. (*A*) Four subdivisions of the DMN; (*B*) four subdivisions of the ECN; (*C*) one subdivision of the SAL; (*D*) four subdivisions of the SMN; (*E*) two subdivisions of the VIS. Each color corresponds to one subdivision. Each subdivision is further described in the supplementary material (Supplementary Table S3 and Supplementary Figure S11).

major spatial differences were localized in the posterior medial temporal lobe—which was part of the DMN from CamCAN35−, but not from Atlas55+ (Fig. 5).

For the ECN, 58% of the network's voxels showed consistency across all three older-adult cohorts. In Atlas55+, the ECN included parts of the dorsolateral prefrontal cortex, the lateral and medial parietal cortex, the posterior inferior temporal cortex, the posterior parahippocampal gyrus and some bilateral cerebellar clusters. The ECN further included four reliable subnetworks comprising the right and left lateral parietal–frontal cortex, as well as two posterior subdivisions mostly covering the posterior parietal lobe and the medial temporal lobe. The whole ECN showed a 60% overlap with the ECN in younger adults as defined in CamCAN35−. The major differences involved the additions of the posterior medial temporal lobe (lingual and parahippocampal gyri) in the ECN from Atlas55+ (Fig. 5).

The SAL network emerged as the least reproducible network: 25% of the network's voxels were consistently assigned to the SAL across the three older-adult cohorts. In Atlas55+, the SAL was comprised of the anterior insula bilaterally, the dorsal ACC, the supramarginal gyri, subcortical regions including the putamen and thalamic nuclei, and bilateral cerebellar clusters. We only found one reliable subdivision which mostly covered the dorsal ACC and supramarginal gyri, bilaterally (Fig. 4). The

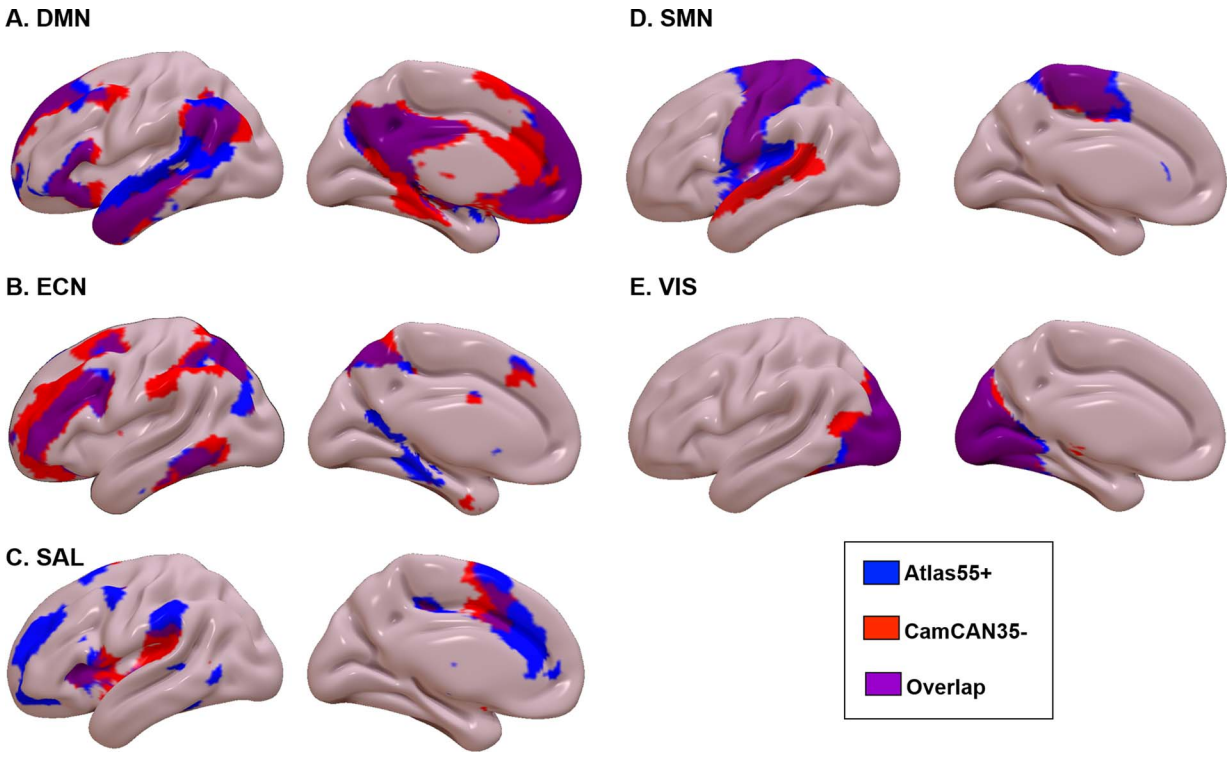

Figure 5. Spatial comparison of the major resting state networks between adults over the age of 55 years, as defined in Atlas55+, and younger adults (aged 18–35 years) from the CamCAN35− cohort.

spatial overlap with the whole SAL in younger adults as defined in CamCAN35− was the lowest with 30% and the regional differences were widespread (Fig. 5).

Associations of Sex and Age with the Spatial Distribution of the Major RSNs in Atlas55+

Sex: we did not find any significant differences between males and females on the spatial distribution of any major RSN in the atlas.

Age: we found a negative regional association with age for each of the major RSNs in the atlas (Fig. 6, Supplementary Table S4). In detail, increasing age was associated with lower spatial integrity of: (1) both anterior and posterior medial regions in the DMN (Fig. 6A), (2) bilateral frontoparietal regions in the ECN (Fig. 6B), (3) bilateral anterior insula and dorsal ACC in the SAL (Fig. 6C), (4) bilateral superior temporal and postcentral gyri in the SMN (Fig. 6D), and to a lesser degree (5) in the calcarine and lingual gyri of the VIS (Fig. 6E).

In contrast, increasing age was associated with higher spatial integrity of cerebellar regions in both the DMN and the ECN (Supplementary Table S4). No other results were significant.

Discussion

This study investigated (1) the spatial definition of the major RSNs in healthy individuals in late adulthood using rs-fMRI data from three large independent cohorts of participants aged 55 years and above and; (2) differences in the spatial definition of RSNs in late adulthood to those derived from healthy individuals in early adulthood. We found a high reproducibility of the spatial definition of the RSNs across the cohorts of older adults, but also significant differences when compared to the RSNs of younger adults. In response to these findings, we constructed Atlas55+, a robust brain functional atlas derived from rs-fMRI of 563 healthy adults between the ages of 55 and 95 years, in order to promote RSN reproducibility in future studies focusing on older populations. The age cutoff of 55 years may be considered arbitrary but there is currently no clear consensus on a specific age that distinguishes middle to late adulthood. In response, we followed the same age criterion as in ADNI, which is a landmark initiative in North America to investigate brain organization in older populations (Jack Jr. et al. 2008; Petersen et al. 2010).

Despite different MRI scanner types, acquisition parameters, and sites, we demonstrated good reproducibility of the spatial definition of the RSNs across the three older-adult cohorts. Regardless of the cohort, the regions with the highest spatial overlap between RSNs were localized in the medial prefrontal cortex, the precuneus, and the lateral parietal cortex, which have been described as brain hubs in young adults (Tomasi & Volkow, 2011; Zuo et al. 2012). Participation in multiple networks is thought to reflect an inherent feature of these associative regions (Yeo et al. 2014). Although studies have reported a negative effect of aging on the strength of these regional hubs (Damoiseaux 2017; Zhang et al. 2017), the current study suggests that the variability in their location remains relatively unaltered within older healthy populations.

Across the three older-adult cohorts, we found that the most reproducible networks were the SMN and VIS networks. These networks are mostly covering primary cortices, which are known to have high structural-functional coherence (Luo et al. 2020a), low interindividual variability in anatomical morphology (White et al. 1997) and in resting-state functional connectivity (Franco et al. 2013; Mueller et al. 2013; Li et al. 2017), and tend to

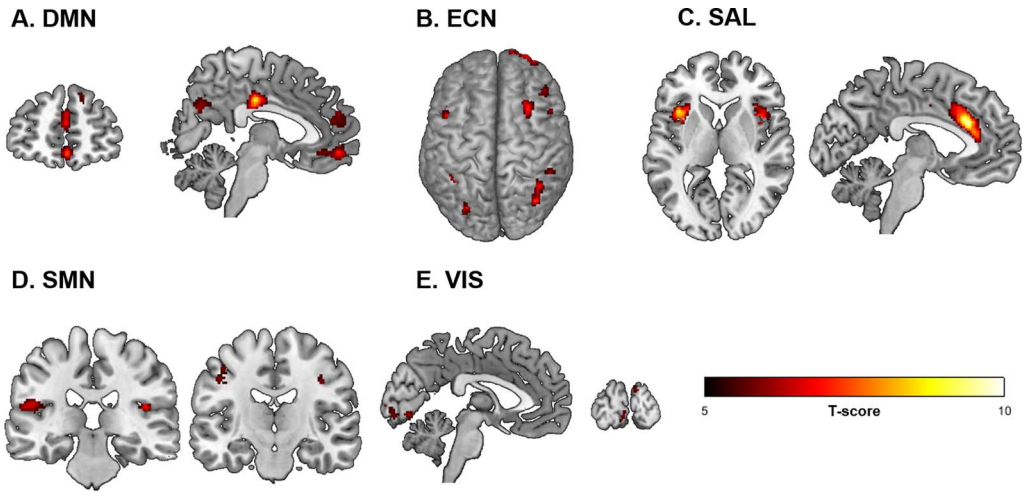

Figure 6. Clusters showing lower spatial integration with the rest of the RSN, with older age, across the three older-adult cohorts. Details of the clusters are in Supplementary Table S3. Significance set up at $P < 0.05$ (FWE correction at the voxel level).

preferentially participate in single networks in line with their circumscribed and specific functions (Yeo et al. 2014). In contrast, the SAL network showed the largest spatial differences across the three older-adult cohorts. This was consistent with the fact that we only identified one reliable subdivision of the SAL, in contrast to the other high-order RSNs (i.e., DMN and ECN) that showed four reliable subdivisions each. In studies of individuals below the age of 40 years, the spatial definition and role of the SAL network have been largely variable (Dosenbach et al. 2007; Seeley et al. 2007; Smith et al. 2009; Yeo et al. 2011; Shirer et al. 2012; Doucet et al. 2019) and this appears to be the case in older adults too.

In line with what we hypothesized, we found age-related alterations in the spatial composition of all five RSNs. The association of RSN spatial definition with age was examined in two different and complementary ways. First, by comparing RSNs between older and younger adults and second by examining the effect of age within the older age-group by testing its association with RSN constitution in the RSNs defined by Atlas55+. Comparison of younger and older adults showed that the SMN and VIS showed the smallest age-related differences, whereas the DMN, ECN and SAL showed the highest degree of age-related spatial reorganization. These findings accord with those of prior studies which have consistently reported that the functional connectivity within networks supporting higher order functions is more affected by age than that of networks supporting lower order functions (Mowinckel et al. 2012; He et al. 2013; Betzel et al. 2014). Also, a recent study by Luo, et al. (2020a) showed more extensive age-related changes in the structural-functional coherence of the associative cortex compared with that of the unimodal cortex. The posterior medial temporal regions—which are typically identified as part of the DMN in younger adults (Buckner et al. 2008; Doucet et al. 2011; Buckner and DiNicola 2019)—were instead assigned to the ECN in the older adults. This finding is in agreement with the notion that cognitive aging involves reorganization rather than loss of function (Reuter-Lorenz and Lustig 2005; Andrews-Hanna et al. 2007; Yaple et al. 2019). This regional variability of the DMN and ECN is also supported by the "the default to executive coupling" model of cognitive aging proposed by Turner and Spreng (2015). This model proposes a regional shift in the architecture of the DMN and ECN to support crystallized cognition in later life (Spreng et al. 2018). We also found large spatial differences in the SAL between the younger and older adults, with the younger adults showing a more restricte network (Seeley et al. 2007). As discussed above, the origin of this large interindividual variability is unclear. Future investigations focusing on the SAL are needed to determine whether the spatial differences may be related to analytical or true biological differences between samples.

We found a significant association of age with the functional integrity of the major RSNs in older adults, particularly in the major regions of the DMN, ECN, and SAL. This finding was expected as the age range across all older participants was 40 years. This was consistent with prior neuroimaging studies that described an effect of aging on both brain structure and function in populations over age 50 (Betzel et al. 2014; Chan et al. 2014; Luis et al. 2015; Damoiseaux 2017; Varangis, Habeck, et al. 2019a; Dima et al. 2020; Frangou et al. 2020; Luo, Sui, Abrol, Lin, et al. 2020b). The overall negative impact of age on each network largely confirms a reduction of functional cohesiveness of the major brain networks, particularly those supporting higher order cognitive functions (Damoiseaux et al. 2008; Mowinckel et al. 2012; He et al. 2013; Betzel et al. 2014; Yaple et al. 2019). It is interesting to note that we also found a positive association of age in cerebellar regions in both the DMN and ECN, suggesting higher cerebellar-cortical integration in these two networks with older age. Zhang et al. (2017) reported similar findings of increased cerebellar-neocortical functional connectivity with age in healthy participants between the age of 12 and 79 years. This higher cerebellar-neocortical integration has also been associated with successful higher order cognitive activity in a healthy elderly population (Luis et al. 2015). Collectively, the findings reported in the current study underscore the importance of age-adapted brain functional atlases.

Moving forward, we propose Atlas55+ that has several advantages to study brain activity in late adulthood. To the best of our knowledge, Atlas55+ (1) is the only atlas based on rs-fMRI datasets from three independent cohorts including a total of 563 healthy participants above the age of 55 years; (2) includes functional partitions of the brain at the level of the large RSNs and their subdivisions; (3) accommodates differences in

neuroimaging acquisition parameters (i.e., different sites, MRI scanners, and acquisition sequences); and (4) is independent of sample composition. We identified 15 reproducible RSN subdivisions (Fig. 4), which is in a typical range for subdivisions reported in brain functional atlases based on younger adults' rs-fMRI data (Yeo et al. 2011; Doucet et al. 2019). We note that the subdivisions reported were those that were identified in all three older-adult cohorts, to minimize potential influences by differences in MRI acquisition parameters. Further studies are needed to confidently identify the exact causes of variation in these subdivisions between the cohorts.

Although Atlas55+ offers a realistic option for standardizing the definition of RSNs for older adults, we acknowledge its limitations. First, the age cutoff of 55 years follows the criterion used in ADNI, which can be viewed as arbitrary. Second, age-related changes in RSN configuration are likely to continue throughout late life and these subtle changes may not be fully captured by Atlas55+. The option of creating brain functional atlases in older individuals to cover specific and smaller time periods (i.e., for every decade past the 55th year) is challenging at present as high-quality rs-fMRI datasets are scarce in older participants, particularly in advanced old age. The Human Connectome Project-Aging dataset may help achieve this goal when it will be fully released (https://www.humanconnectome.org/study/hcp-lifespan-aging). Third, we constructed Atlas55+ using a volumetric-based (ICA) rather than a surface-based approach. We previously demonstrated that MICCA provided reliable networks (Naveau et al. 2012), and the analytic approach does not significantly alter the reproducibility of the RSNs as long as they are derived from a sample of at least 100 individuals (Doucet et al. 2019), which is the case for each cohort analyzed in the current study. Therefore, it is unlikely that this choice strongly influenced the spatial definition of the RSNs. Fourth, we focused on the five major RSNs (DMN, ECN, SAL, SMN, VIS) and their subdivisions as these are the most reproducible networks in the neuroimaging literature (van den Heuvel and Hulshoff Pol 2010; Doucet et al. 2019; Elliott et al. 2019). As aging is associated with reduced brain modularity (Meunier et al. 2009; Damoiseaux 2017; Varangis, Razlighi, et al. 2019b), we cannot exclude the possibility that the clustering approach did not influence the current findings (Abou Elseoud et al. 2011). However, each of these five RSNs have been consistently identified in aging studies (Damoiseaux et al. 2008; Mowinckel et al. 2012; Betzel et al. 2014; Sala-Llonch et al. 2015; Varangis, Habeck, et al. 2019a), suggesting that their existence in older individuals is indisputable. Lastly, this study specifically focused on the spatial characteristics of the RSNs; other characteristics such as their dynamics or the association with cognitive variability in late adulthood were not explored because the necessary data were not available. In particular, it will be important to investigate the cognitive impact on the spatial definition of the Atlas55+ RSNs, in cognitively impaired populations. In the current study, all individuals were identified as healthy and showed very low variability in their general functioning (Mini-mental state exam score: mean (std): 28.6 (1.5), across the CamCAN55+ and ADNI cohorts) which prevented further analyses to identify spatial variability in the RSNs as a function of cognitive ability.

Conclusion

We presented a quantitative comparison of the spatial composition of the major RSNs and their reliable functional subdivisions derived from healthy adults between the ages of 55 and 95 years old and younger adults aged 18–35 years. We also identified the spatial distribution of age-related changes in RSN definition. Our results confirm the importance of age-appropriate brain functional atlases for studies investigating brain mechanisms related to aging. We propose that Atlas55+ can provide a reproducible template of the major RSNs for late adulthood as it is publicly available (https://www.researchgate.net/project/Brain-functional-organization).

Supplementary Material

Supplementary material can be found at *Cerebral Cortex* online.

Funding

National Institute of Aging (R03AG064001 to G.E.D); the National Institute of General Medical Sciences (P20GM130447 to G.E.D.); the National Institute of Mental Health (R01MH113619 to S.F); the National Institute of Biomedical Imaging and Bioengineering (U54 EB020403 to P.M.T.); the French government agency ANR (LABCOM Ginesislab, ANR 16-LCV2-0006-01 to M.J.). French Alternative Energies and Atomic Energy Commission (L.L. through fellowship). Alzheimer's Disease Neuroimaging Initiative (ADNI) (National Institutes of Health Grant U01 AG024904 for data collection and sharing) and DOD ADNI (Department of Defense award number W81XWH-12-2-0012). National Institute on Aging (A.D.N.I.), the National Institute of Biomedical Imaging and Bioengineering (A.D.N.I.), and generous contributions to A.D.N.I. from the following: AbbVie, Alzheimer's Association; Alzheimer's Drug Discovery Foundation; Araclon Biotech; BioClinica, Inc.; Biogen; Bristol-Myers Squibb Company; CereSpir, Inc.; Cogstate; Eisai Inc.; Elan Pharmaceuticals, Inc.; Eli Lilly and Company; EuroImmun; F. Hoffmann-La Roche Ltd and its affiliated company Genentech, Inc.; Fujirebio; GE Healthcare; IXICO Ltd; Janssen Alzheimer Immunotherapy Research & Development, LLC.; Johnson & Johnson Pharmaceutical Research & Development LLC.; Lumosity; Lundbeck; Merck & Co., Inc.; Meso Scale Diagnostics, LLC.; NeuroRx Research; Neurotrack Technologies; Novartis Pharmaceuticals Corporation; Pfizer Inc.; Piramal Imaging; Servier; Takeda Pharmaceutical Company; and Transition Therapeutics. The Canadian Institutes of Health Research is providing funds to support A.D.N.I. clinical sites in Canada. Private sector contributions are facilitated by the Foundation for the National Institutes of Health (www.fnih.org).

Notes

The grantee organization is the Northern California Institute for Research and Education, and the study is coordinated by the Alzheimer's Therapeutic Research Institute at the University of Southern California. ADNI data are disseminated by the Laboratory for Neuro Imaging at the University of Southern California. *Conflict of Interest:* None declared.

Data and Code Availability

The datasets used in the current study are freely available or upon request (links provided in supplementary material). The RSNs extracted for each cohort and from Atlas55+ are available (https://www.researchgate.net/project/Brain-functional-organization) and upon request to the corresponding author.

References

Abou Elseoud A, Littow H, Remes J, Starck T, Nikkinen J, Nissila J, Timonen M, Tervonen O, Kiviniemi V. 2011. Group-ICA model order highlights patterns of functional brain connectivity. *Front Syst Neurosci*. 5:37.

Andrews-Hanna JR, Snyder AZ, Vincent JL, Lustig C, Head D, Raichle ME, Buckner RL. 2007. Disruption of large-scale brain systems in advanced aging. *Neuron*. 56:924–935.

Beckmann CF, Mackay CE, Filippini N, Smith SM, 2009. Group comparison of resting-state fMRI data using multi-subject ICA and dual regression. *Organ Hum Brain Mapp*.

Beckmann CF, Smith SM. 2004. Probabilistic independent component analysis for functional magnetic resonance imaging. *IEEE Trans Med Imaging*. 23:137–152.

Behzadi Y, Restom K, Liau J, Liu TT. 2007. A component based noise correction method (CompCor) for BOLD and perfusion based fMRI. *Neuroimage*. 37:90–101.

Betzel RF, Byrge L, He Y, Goni J, Zuo XN, Sporns O. 2014. Changes in structural and functional connectivity among resting-state networks across the human lifespan. *Neuroimage*. 102(Pt 2):345–357.

Bijsterbosch JD, Woolrich MW, Glasser MF, Robinson EC, Beckmann CF, Van Essen DC, Harrison SJ, Smith SM. 2018. The relationship between spatial configuration and functional connectivity of brain regions. *Elife*. 7:e32992.

Buckner RL, Andrews-Hanna JR, Schacter DL. 2008. The brain's default network: anatomy, function, and relevance to disease. *Ann N Y Acad Sci*. 1124:1–38.

Buckner RL, DiNicola LM. 2019. The brain's default network: updated anatomy, physiology and evolving insights. *Nat Rev Neurosci*. 20:593–608.

Buckner RL, Krienen FM, Yeo BT. 2013. Opportunities and limitations of intrinsic functional connectivity MRI. *Nat Neurosci*. 16:832–837.

Buckner RL, Sepulcre J, Talukdar T, Krienen FM, Liu H, Hedden T, Andrews-Hanna JR, Sperling RA, Johnson KA. 2009. Cortical hubs revealed by intrinsic functional connectivity: mapping, assessment of stability, and relation to Alzheimer's disease. *Journal of Neurosci*. 29:1860–1873.

Chan MY, Park DC, Savalia NK, Petersen SE, Wig GS. 2014. Decreased segregation of brain systems across the healthy adult lifespan. *Proc Natl Acad Sci USA*. 111:E4997–E5006.

Cordes D, Haughton VM, Arfanakis K, Carew JD, Turski PA, Moritz CH, Quigley MA, Meyerand ME. 2001. Frequencies contributing to functional connectivity in the cerebral cortex in "resting-state" data. *AJNR Am J Neuroradiol*. 22:1326–1333.

Damoiseaux JS. 2017. Effects of aging on functional and structural brain connectivity. *Neuroimage*. 160:32–40.

Damoiseaux JS, Beckmann CF, Arigita EJ, Barkhof F, Scheltens P, Stam CJ, Smith SM, Rombouts SA. 2008. Reduced resting-state brain activity in the "default network" in normal aging. *Cereb Cortex*. 18:1856–1864.

Damoiseaux JS, Rombouts SA, Barkhof F, Scheltens P, Stam CJ, Smith SM, Beckmann CF. 2006. Consistent resting-state networks across healthy subjects. *Proc Natl Acad Sci USA*. 103:13848–13853.

De Luca M, Beckmann CF, De Stefano N, Matthews PM, Smith SM. 2006. fMRI resting state networks define distinct modes of long-distance interactions in the human brain. *Neuroimage*. 29:1359–1367.

Dice LR. 1945. Measures of the amount of ecologic association between species. *Ecology*. 26:297–302.

Dima D, Papachristou E, Modabbernia A, Doucet GE, Agartz I, Aghajani M, Akudjedu TN, Albajes-Eizagirre A, Alnæs D, Alpert KI. 2020. Subcortical Volume Trajectories across the Lifespan: Data from 18,605 healthy individuals aged 3-90 years. *bioRxiv*. 2020.05.05.079475. doi: https://doi.org/10.1101/2020.05.05.079475.

Dong D, Wang Y, Chang X, Luo C, Yao D. 2018. Dysfunction of large-scale brain networks in schizophrenia: a meta-analysis of resting-state functional connectivity. *Schizophr Bull*. 44:168–181.

Dosenbach NU, Fair DA, Miezin FM, Cohen AL, Wenger KK, Dosenbach RA, Fox MD, Snyder AZ, Vincent JL, Raichle ME *et al*. 2007. Distinct brain networks for adaptive and stable task control in humans. *Proc Natl Acad Sci USA*. 104:11073–11078.

Doucet G, Naveau M, Petit L, Delcroix N, Zago L, Crivello F, Jobard G, Tzourio-Mazoyer N, Mazoyer B, Mellet E *et al*. 2011. Brain activity at rest: a multiscale hierarchical functional organization. *J Neurophysiol*. 105:2753–2763.

Doucet G, Naveau M, Petit L, Zago L, Crivello F, Jobard G, Delcroix N, Mellet E, Tzourio-Mazoyer N, Mazoyer B *et al*. 2012. Patterns of hemodynamic low-frequency oscillations in the brain are modulated by the nature of free thought during rest. *Neuroimage*. 59:3194–3200.

Doucet GE, Bassett DS, Yao N, Glahn DC, Frangou S. 2017. The role of intrinsic brain functional connectivity in vulnerability and resilience to bipolar disorder. *Am J Psychiatry*. 174:1214–1222.

Doucet GE, Lee WH, Frangou S. 2019. Evaluation of the spatial variability in the major resting-state networks across human brain functional atlases. *Hum Brain Mapp*. 40:4577–4587.

Elliott ML, Knodt AR, Cooke M, Kim MJ, Melzer TR, Keenan R, Ireland D, Ramrakha S, Poulton R, Caspi A *et al*. 2019. General functional connectivity: shared features of resting-state and task fMRI drive reliable and heritable individual differences in functional brain networks. *Neuroimage*. 189:516–532.

Feltz CJ, Miller GE. 1996. An asymptotic test for the equality of coefficients of variation from k populations. *Stat Med*. 15:646–658.

Fox MD, Snyder AZ, Vincent JL, Corbetta M, Van Essen DC, Raichle ME. 2005. The human brain is intrinsically organized into dynamic, anticorrelated functional networks. *Proc Natl Acad Sci USA* 102:9673–9678.

Franco AR, Mannell MV, Calhoun VD, Mayer AR. 2013. Impact of analysis methods on the reproducibility and reliability of resting-state networks. *Brain Connect*. 3:363–374.

Frangou S, Modabbernia A, Doucet GE, Papachristou E, Williams SCR, Agartz I, Aghajani M, Akudjedu TN, Albajes-Eizagirre A, Alnæs D *et al*.. 2020. Cortical Thickness Trajectories across the Lifespan: Data from 17,075 healthy individuals aged 3-90 years. *bioRxiv*. 2020.05.05.077834; doi: https://doi.org/10.1101/2020.05.05.077834.

Friston KJ, Williams S, Howard R, Frackowiak RS, Turner R. 1996. Movement-related effects in fMRI time-series. *Magn Reson Med*. 35:346–355.

Greicius MD, Supekar K, Menon V, Dougherty RF. 2009. Resting-state functional connectivity reflects structural connectivity in the default mode network. *Cereb Cortex*. 19:72–78.

He X, Qin W, Liu Y, Zhang X, Duan Y, Song J, Li K, Jiang T, Yu C. 2013. Age-related decrease in functional connectivity of the right fronto-insular cortex with the central executive and default-mode networks in adults from young to middle age. *Neurosci Lett*. 544:74–79.

Himberg J, Hyvarinen A, Esposito F. 2004. Validating the independent components of neuroimaging time series via clustering and visualization. *Neuroimage*. 22:1214–1222.

Hyvarinen A. 1999. Fast and robust fixed-point algorithms for independent component analysis. *IEEE Trans Neural Netw*. 10:626–634.

Jack CR Jr, Bernstein MA, Fox NC, Thompson P, Alexander G, Harvey D, Borowski B, Britson PJ, Whitwell JL, Ward C *et al*. 2008. The Alzheimer's disease neuroimaging initiative (ADNI): MRI methods. *J Magn Reson Imaging*. 27:685–691.

Kiviniemi V, Starck T, Remes J, Long X, Nikkinen J, Haapea M, Veijola J, Moilanen I, Isohanni M, Zang YF *et al*. 2009. Functional segmentation of the brain cortex using high model order group PICA. *Hum Brain Mapp*. 30:3865–3886.

Labache L, Joliot M, Saracco J. 2020. Study of the inter-individual variability of intrinsic connectivity data: detection of unstable networks and sub-populations in a three-dimensional tablearXiv preprint. arXiv:2004.05033. 29 September 2020, preprint: not peer reviewed.

Li R, Yin S, Zhu X, Ren W, Yu J, Wang P, Zheng Z, Niu YN, Huang X, Li J. 2017. Linking inter-individual variability in functional brain connectivity to cognitive ability in elderly individuals. *Front Aging Neurosci*. 9:385.

Luis EO, Arrondo G, Vidorreta M, Martinez M, Loayza F, Fernandez-Seara MA, Pastor MA. 2015. Successful working memory processes and cerebellum in an elderly sample: a neuropsychological and fMRI study. *PLoS One*. 10:e0131536.

Luo N, Sui J, Abrol A, Chen J, Turner JA, Damaraju E, Fu Z, Fan L, Lin D, Zhuo C *et al*. 2020a. Structural brain architectures match intrinsic functional networks and vary across domains: a study from 15 000+ individuals. *Cereb Cortex*. 30:5460–5470.

Luo N, Sui J, Abrol A, Lin D, Chen J, Vergara VM, Fu Z, Du Y, Damaraju E, Xu Y *et al*. 2020b. Age-related structural and functional variations in 5,967 individuals across the adult lifespan. *Hum Brain Mapp*. 41:1725–1737.

Meunier D, Achard S, Morcom A, Bullmore E. 2009. Age-related changes in modular organization of human brain functional networks. *Neuroimage*. 44:715–723.

Minka T. 2000. Automatic choice of dimensionality for PCA. Technical Report 514, MIT Media Lab.

Mowinckel AM, Espeseth T, Westlye LT. 2012. Network-specific effects of age and in-scanner subject motion: a resting-state fMRI study of 238 healthy adults. *Neuroimage*. 63:1364–1373.

Mueller S, Wang D, Fox MD, Yeo BT, Sepulcre J, Sabuncu MR, Shafee R, Lu J, Liu H. 2013. Individual variability in functional connectivity architecture of the human brain. *Neuron*. 77:586–595.

Naveau M, Doucet G, Delcroix N, Petit L, Zago L, Crivello F, Jobard G, Mellet E, Tzourio-Mazoyer N, Mazoyer B *et al*. 2012. A novel group ICA approach based on multi-scale individual component clustering. Application to a large sample of fMRI data. *Neuroinformatics*. 10:269–285.

Nickerson LD, Smith SM, Ongur D, Beckmann CF. 2017. Using dual regression to investigate network shape and amplitude in functional connectivity analyses. *Front Neurosci*. 11:115.

Patel AX, Kundu P, Rubinov M, Jones PS, Vertes PE, Ersche KD, Suckling J, Bullmore ET. 2014. A wavelet method for modeling and despiking motion artifacts from resting-state fMRI time series. *Neuroimage*. 95:287–304.

Petersen RC, Aisen PS, Beckett LA, Donohue MC, Gamst AC, Harvey DJ, Jack CR Jr, Jagust WJ, Shaw LM, Toga AW *et al*. 2010. Alzheimer's disease neuroimaging initiative (ADNI): clinical characterization. *Neurology*. 74:201–209.

Power JD, Barnes KA, Snyder AZ, Schlaggar BL, Petersen SE. 2012. Spurious but systematic correlations in functional connectivity MRI networks arise from subject motion. *Neuroimage*. 59:2142–2154.

Reuter-Lorenz PA, Lustig C. 2005. Brain aging: reorganizing discoveries about the aging mind. *Curr Opin Neurobiol*. 15:245–251.

Sala-Llonch R, Bartres-Faz D, Junque C. 2015. Reorganization of brain networks in aging: a review of functional connectivity studies. *Front Psychol*. 6:663.

Salman MS, Du Y, Lin D, Fu Z, Fedorov A, Damaraju E, Sui J, Chen J, Mayer AR, Posse S *et al*. 2019. Group ICA for identifying biomarkers in schizophrenia: 'Adaptive' networks via spatially constrained ICA show more sensitivity to group differences than spatio-temporal regression. *Neuroimage Clin*. 22:101747.

Seeley WW, Menon V, Schatzberg AF, Keller J, Glover GH, Kenna H, Reiss AL, Greicius MD. 2007. Dissociable intrinsic connectivity networks for salience processing and executive control. *J Neurosci*. 27:2349–2356.

Sha Z, Wager TD, Mechelli A, He Y. 2019. Common dysfunction of large-scale neurocognitive networks across psychiatric disorders. *Biol Psychiatry*. 85:379–388.

Shafto MA, Tyler LK, Dixon M, Taylor JR, Rowe JB, Cusack R, Calder AJ, Marslen-Wilson WD, Duncan J, Dalgleish T *et al*. 2014. The Cambridge Centre for Ageing and Neuroscience (Cam-CAN) study protocol: a cross-sectional, lifespan, multidisciplinary examination of healthy cognitive ageing. *BMC Neurol*. 14:204.

Shirer WR, Ryali S, Rykhlevskaia E, Menon V, Greicius MD. 2012. Decoding subject-driven cognitive states with whole-brain connectivity patterns. *Cereb Cortex*. 22: 158–165.

Smith SM, Fox PT, Miller KL, Glahn DC, Fox PM, Mackay CE, Filippini N, Watkins KE, Toro R, Laird AR *et al*. 2009. Correspondence of the brain's functional architecture during activation and rest. *Proc Natl Acad Sci USA*. 106:13040–13045.

Smith SM, Jenkinson M, Woolrich MW, Beckmann CF, Behrens TE, Johansen-Berg H, Bannister PR, De Luca M, Drobnjak I, Flitney DE *et al*. 2004. Advances in functional and structural MR image analysis and implementation as FSL. *Neuroimage*. 23(Suppl 1):S208–S219.

Smith SM, Nichols TE, Vidaurre D, Winkler AM, Behrens TE, Glasser MF, Ugurbil K, Barch DM, Van Essen DC, Miller KL. 2015. A positive-negative mode of population covariation links brain connectivity, demographics and behavior. *Nat Neurosci*. 18:1565–1567.

Spreng RN, Lockrow AW, DuPre E, Setton R, Spreng KAP, Turner GR. 2018. Semanticized autobiographical memory and the default - executive coupling hypothesis of aging. *Neuropsychologia*. 110:37–43.

Taylor JR, Williams N, Cusack R, Auer T, Shafto MA, Dixon M, Tyler LK, Cam C, Henson RN. 2017. The Cambridge Centre for Ageing and Neuroscience (Cam-CAN) data repository: structural and functional MRI, MEG, and cognitive data from a cross-sectional adult lifespan sample. *Neuroimage*. 144:262–269.

Tomasi D, Volkow ND. 2011. Association between functional connectivity hubs and brain networks. *Cereb Cortex*. 21:2003–2013. doi: 10.1093/cercor/bhq268.

Toosy AT, Ciccarelli O, Parker GJ, Wheeler-Kingshott CA, Miller DH, Thompson AJ. 2004. Characterizing function-structure relationships in the human visual system with functional MRI and diffusion tensor imaging. *Neuroimage*. 21:1452–1463.

Tracy JI, Doucet GE. 2015. Resting-state functional connectivity in epilepsy: growing relevance for clinical decision making. *Curr Opin Neurol*. 28:158–165.

Turner GR, Spreng RN. 2015. Prefrontal engagement and reduced default network suppression co-occur and are dynamically coupled in older adults: the default-executive coupling hypothesis of aging. *J Cogn Neurosci*. 27:2462–2476.

van den Heuvel MP, Hulshoff Pol HE. 2010. Exploring the brain network: a review on resting-state fMRI functional connectivity. *Eur Neuropsychopharmacol*. 20:519–534.

van den Heuvel MP, Mandl RC, Kahn RS, Hulshoff Pol HE. 2009. Functionally linked resting-state networks reflect the underlying structural connectivity architecture of the human brain. *Hum Brain Mapp*. 30:3127–3141.

Varangis E, Habeck CG, Razlighi QR, Stern Y. 2019a. The effect of aging on resting state connectivity of predefined networks in the brain. *Front Aging Neurosci*. 11:234.

Varangis E, Razlighi Q, Habeck CG, Fisher Z, Stern Y. 2019b. Between-network functional connectivity is modified by age and cognitive task domain. *J Cogn Neurosci*. 31: 607–622.

Wei D, Zhuang K, Ai L, Chen Q, Yang W, Liu W, Wang K, Sun J, Qiu J. 2018. Structural and functional brain scans from the cross-sectional Southwest University adult lifespan dataset. *Sci Data*. 5:180134.

White LE, Andrews TJ, Hulette C, Richards A, Groelle M, Paydarfar J, Purves D. 1997. Structure of the human sensorimotor system. I: morphology and cytoarchitecture of the central sulcus. *Cereb Cortex*. 7:18–30.

Yan CG, Wang XD, Zuo XN, Zang YF. 2016. DPABI: data processing & analysis for (resting-state) brain imaging. *Neuroinformatics*. 14:339–351.

Yaple ZA, Stevens WD, Arsalidou M. 2019. Meta-analyses of the n-back working memory task: fMRI evidence of age-related changes in prefrontal cortex involvement across the adult lifespan. *Neuroimage*. 196:16–31.

Yeo BT, Krienen FM, Chee MW, Buckner RL. 2014. Estimates of segregation and overlap of functional connectivity networks in the human cerebral cortex. *Neuroimage*. 88:212–227.

Yeo BT, Krienen FM, Sepulcre J, Sabuncu MR, Lashkari D, Hollinshead M, Roffman JL, Smoller JW, Zollei L, Polimeni JR *et al*. 2011. The organization of the human cerebral cortex estimated by intrinsic functional connectivity. *J Neurophysiol*. 106:1125–1165.

Zalesky A, Fornito A, Harding IH, Cocchi L, Yucel M, Pantelis C, Bullmore ET. 2010. Whole-brain anatomical networks: does the choice of nodes matter? *Neuroimage*. 50:970–983.

Zhang H, Lee A, Qiu A. 2017. A posterior-to-anterior shift of brain functional dynamics in aging. *Brain Struct Funct*. 222: 3665–3676.

Zuo XN, Ehmke R, Mennes M, Imperati D, Castellanos FX, Sporns O, Milham MP. 2012. Network centrality in the human functional connectome. *Cereb Cortex*. 22:1862–1875. doi: 10.1093/cercor/bhr269.